

From Zero-Intelligence to Queue-Reactive:
Limit-Order-Book modeling for high-frequency volatility
estimation and optimal execution

Tommaso Mariotti

Scuola Normale Superiore

`tommaso.mariotti@sns.it`

Fabrizio Lillo

University of Bologna and Scuola Normale Superiore

`fabrizio.lillo@unibo.it`

Giacomo Toscano

University of Firenze

`giacomo.toscano@unifi.it`

September 20, 2022

Abstract

The estimation of the volatility of financial assets with high-frequency data is plagued by the presence of microstructure noise, which leads to biased measures. Alternative estimators have been developed and tested either on specific structures of the noise or by the speed of convergence to their asymptotic error distributions. Gatheral and Oomen (2010) proposed to use the Zero-Intelligence model of the limit order book to test the finite-sample performance of several estimators of the integrated variance. Building on this approach, in this paper we introduce three main innovations: (i) we use as data-generating process the Queue-Reactive model

of the limit order book (Huang et al. (2015)), which - compared to the Zero-Intelligence model - generates more realistic microstructure dynamics, as shown here by means of the Hausman test by Aït-Sahalia and Xiu (2019); (ii) we consider not only estimators of the integrated volatility but also of the spot volatility; (iii) we show the relevance of the estimator in the prediction of the variance of the cost of a simulated VWAP execution. In the case of the integrated volatility, we find that the pre-averaging estimator optimizes the estimation bias, while the unified and alternation estimators lead to optimal mean squared error values. Instead, in the case of the spot volatility, the Fourier estimator yields the optimal accuracy, both in terms of bias and mean squared error. The latter estimator leads also to the optimal prediction of the cost variance of a VWAP execution.

1 Introduction

The availability of efficient estimates of the volatility of financial assets is crucial for a number of applications, such as model calibration, risk management, derivatives pricing, high-frequency trading and optimal execution. High-frequency data provide, in principle, the possibility of obtaining very precise estimates of the volatility. The (infill) asymptotic theory of volatility estimators was initially derived under the assumption that the asset price follows an Itô semimartingale (see Chapter 3 of Aït-Sahalia and Jacod (2014)). The Itô semimartingale hypothesis ensures the absence of arbitrage opportunities (see Delbaen and Schachermayer (1994)) and, at the same time, is rather flexible, as it does not require to specify any parametric form for the dynamics of the asset price.

However, empirical evidences and theoretical motivations indicate that the prices of financial assets do not conform to the semimartingale hypothesis at high frequencies, due to the presence of microstructure phenomena such as, e.g., bid-ask bounces or price rounding (see Hasbrouck (2007) for a review). From the statistical point of view, such phenomena have been modeled as an additive noise component and the asymptotic theory that takes into account the presence of the latter was readily developed (see Chapter 7 of Aït-Sahalia and Jacod (2014)). In its most basic form, the noise due to microstructure is assumed to be i.i.d. and independent of the semimartingale driving the price dynamics (i.e., the so-called efficient price). Moreover, more sophisticated forms have been studied, such as, for instance, an additive noise which is auto-correlated or correlated with the efficient price (see, e.g., Hansen and Lunde (2006)).

The literature on the estimation of the volatility in the presence of noise is very rich. In fact, there exists a number of alternative methodologies making an efficient use of high-frequency prices to reconstruct not only the total volatility accumulated over a fixed time horizon, i.e., the integrated volatility, but also the trajectory of the latter on a discrete grid, i.e., the spot volatility. These include the two-scale and multi-scale approach by, respectively, L. Zhang et al. (2005) and L. Zhang (2006), the kernel-based method, originally proposed in Barndorff-Nielsen et al. (2008), the Fourier-transform method by Malliavin and Mancino (2002, 2009), and the pre-averaging approach by Jacod et al. (2009). Given this variety of alternative methodologies, it is not straightforward to establish

which specific noise-robust estimator should be preferred for high-frequency financial applications.

As pointed out in the seminal paper by Gatheral and Oomen (2010), the best asymptotic properties, i.e., the optimal rate of convergence and the minimum asymptotic error variance, do not guarantee the best performance in finite-sample applications. Gatheral and Oomen (2010) proposed to compare the finite-sample performance of different high-frequency estimators via simulations based on a market simulator which is able to reproduce the actual mechanism of price formation at high frequencies with sufficient realism. In this regard, the authors used simulations obtained via the Zero-Intelligence (ZI) limit order book model by Smith et al. (2003) to compare the performance of different integrated volatility estimators. However, the ZI model is based on several simplistic assumptions on the dynamics of the limit order book, and thus it may fail to replicate the actual behavior of high frequency financial data and microstructure noise with satisfactory accuracy. For example, under the ZI model, the order flow is described by independent Poisson processes, while it is well-known that the order flow is a long-memory process (see Lillo and Farmer (2004)) and the different components of the order flow are lead-lag cross-correlated (Eisler et al. (2012)). Moreover, as pointed out by Bouchaud et al. (2018), the ZI model leads to systematically profitable market making strategies. These properties are likely to have an effect on the dynamics of the volatility and market microstructure noise, and thus an analysis based on a more realistic limit order book model is needed.

The first goal of this paper is to extend the study by Gatheral and Oomen (2010) in two directions. First, we use a more realistic limit order book model, namely the Queue-Reactive (QR) model by Huang et al. (2015). Under this model, the arrival rates of orders depend on the state of the limit order book. This implicitly introduces auto- and cross-correlations of the book components, thereby generating more realistic dynamics for the price process at high-frequencies. Secondly, we compare not only the performance of a number of estimators of the integrated volatility (expanding the collection of estimators considered in the study by Gatheral and Oomen (2010)), but also that of different estimators of the spot volatility. To make our comparison meaningful for applications, the performance of the estimators is evaluated in terms of the optimization of the bias and the mean-squared-error via the feasible selection of the tuning parameters involved in their implementation. Note that, following Gatheral and Oomen (2010), we consider three alternative price series for the estimation: the mid-price, that is, the average between the best bid and best ask quotes; the micro-price, i.e., the volume-weighted average of the best bid and best ask quotes; the trade price, namely the price at which a market order is executed.

For what concerns the integrated variance, we find that the pre-averaging estimator by Jacod et al. (2009) is favorable in terms of bias minimization. Instead, when looking at the optimization of the mean squared error, the situation appears to be more nuanced. Indeed, the Fourier estimator by Malliavin and Mancino (2009) obtains the best average ranking across the considered price series (mid-, micro- and trade- prices) without actually achieving the best ranking for any of these individual series. The best rankings are instead achieved by the unified volatility estimator by Y. Li,

Z. Zhang, et al. (2018) (for mid- and micro-prices) and by the alternation estimator by Large (2011) (for trade-prices). Instead, for what concerns the spot variance, the Fourier estimator provides the relative best performance for the three prices series, both in terms of bias and mean-squared-error optimization.

The second goal of the paper is to study the impact of the availability of efficient volatility estimates on optimal execution. Specifically, we investigate, via simulations of the QR model, how the use of different volatility estimators affects the inference of the variance of the cost of the execution strategy. To do so, we consider the instance where the trader is set to execute a volume-weighted average price (VWAP) strategy and assumes that market impact is described by the Almgren and Chriss (Almgren and Chriss (2001)) model. We compare the empirical variance of the implementation shortfall of the simulated executions with the corresponding model-based prediction, evaluated with different spot volatility estimators. As a result, we find that the estimator that yields the optimal performance in terms of bias and mean-squared-error optimization, namely the Fourier estimator, also gives the optimal forecast of the cost variance. More generally, our results suggest that the choice of the spot estimator is not irrelevant, as it may lead to significantly different forecasts of the variance of the implementation shortfall.

The paper is organized as follows. In Section 2 we recall the main characteristics of the ZI and QR limit-order-book models, discuss their calibration on empirical data and compare their ability to reproduce realistic volatility and noise features. In Section 3 we illustrate the estimators of the integrated and spot variance, while in Section 4 we evaluate their finite-sample performance with simulated data from the QR model. Finally, Section 5 contains the study of the impact of efficient volatility estimates on optimal execution. Section 6 concludes.

2 Limit-order-book models: zero-intelligence vs queue-reactive

Electronic financial markets are often based on a double auction mechanism, with a bid (buy) side and an ask (sell) side. The limit order book (LOB) is the collection of all the outstanding limit orders, which are orders of buying or selling a given quantity of the asset at a given price, expressed as a multiple of the tick size (i.e., the minimum price movement allowed) of the asset. Other two types of orders can be placed: a cancellation, that erases a limit order previously inserted by the same agent, thereby reducing the volume at a given price level, and a market order, that is, an order to immediately buy/sell the asset at the best possible price. The best bid is the highest price at which there is a limit order to buy, and the best ask is the lowest price at which there is a limit order to sell. The spread is the difference between the best ask and the best bid, and is typically expressed in tick size. For a detailed overview of the LOB see Abergel et al. (2016).

In the following, we will be interested in three price series that can be retrieved from LOB data: the mid-price, the micro-price and the trade price.

Definition 1. *We define the mid-price p_{mid} and the micro-price p_{micro} of an asset at time t as,*

respectively, the arithmetic average and the volume-weighted average of the best bid and best ask quotes at time t , i.e.,

$$p_{mid}(t) := \frac{p^b(t) + p^a(t)}{2}, \quad p_{micro}(t) := \frac{p^b(t)v^a(t) + p^a(t)v^b(t)}{v^b(t) + v^a(t)},$$

where p^b , p^a , v^b and v^a denote, respectively, the best bid, the best ask, the volume (i.e., the number of outstanding limit orders) at the best bid and the volume at the best ask. Finally, the trade price p_{trade} series is defined as the series of prices arising from the execution of market orders.

In our study, we will consider two models for the simulation of the LOB. The simplistic ZI model by Smith et al. (2003) and the more sophisticated QR model by Huang et al. (2015). In the next subsections we briefly recall the main characteristics of the two models. Please refer to the original papers for a more thorough description.

2.1 Model descriptions

The zero-intelligence model

The ZI model, originally proposed by Smith et al. (2003), is a statistical representation of the double action mechanism used in most stock markets. Despite its simplicity, the model is able to generate a relatively complex dynamic for the order book. It is based on three parameters: the intensity of limit orders, λ^L , the intensity of cancel orders, λ^C , and the intensity of market orders, λ^M . The three components of the order flow follow independent Poisson processes, thus the type of order extracted at each time is independent of the previous orders and the current state of the LOB, and orders may arrive at every price level with the same probability. Each order is assumed to have unitary size. For a detailed discussion about the flexibility of this model, see Gatheral and Oomen (2010).

As mentioned, the ZI model may be deemed as too simplistic. Indeed, the assumptions that the intensities of order arrival are independent of the state of the book and that the intensities are equal for each price level are highly unrealistic. Moreover, this model produces purely endogenous order-book dynamics, without considering the effect of exogenous information. Further, as shown in Bouchaud et al. (2018), under the ZI model the market impact of new orders is such that profitable market-making opportunities can be created, even if they are usually absent in real markets. Some of the weakness of the ZI model are overcome by the QR model.

The queue-reactive model

The QR model (Huang et al. (2015)) is a LOB model suitable to describe large tick assets, i.e., assets whose bid-ask spread is almost always equal to one tick. This model is able to reproduce a richer and more realistic behavior of the LOB, compared to the ZI model. In other words, the QR model attempts to fix some of the flaws of the ZI model. This is achieved, in the first place, by

assuming different intensities for each level of the LOB. Moreover, the degree of realism is increased by introducing a correlation not only between order-arrival intensities and the corresponding queue size at each level, but also between intensities and the queue size at the corresponding level at the opposite side of the book. Further, a dependence between the volume at the best level and order arrivals at the other levels is assumed. Finally, differently from the ZI model, the QR model allows for exogenous dynamics by taking into account the flow of exogenous information that hits the market.

Following Huang et al. (2015), under the QR model the LOB is described by a $2K$ -dimensional vector, with K denoting the number of available price levels at the bid and ask sides of the book. At the level $Q_{\pm i}$, $i = 1, \dots, K$, the corresponding price is equal to $p \pm i(\text{tick})$, where p denotes the center of the $2K$ dimensional vector. Precisely, Q_{-i} denotes a level order at the bid side and Q_i denotes a level order at the ask side. Moreover, $q_{\pm i}$ denotes the volume at the level $Q_{\pm i}$.

The process $X(t) = (q_{-K}(t), \dots, q_{-1}(t), q_1(t), \dots, q_K(t))$ is a continuous-time Markov process with the following infinitesimal generator matrix \mathcal{Q} :

$$\begin{aligned} \mathcal{Q}_{q, q+e_i} &= f_i(q), \\ \mathcal{Q}_{q, q-e_i} &= g_i(q), \\ \mathcal{Q}_{q, q} &= -\sum_{p \neq q} \mathcal{Q}_{q, p}, \\ \mathcal{Q}_{q, q} &= 0 \quad \text{otherwise,} \end{aligned}$$

with $q = (q_{-K}, \dots, q_{-1}, q_1, \dots, q_K)$ and e_i denoting the i -th vector of the standard base of \mathbb{R}^{2K} .

Thus, with different intensities at each queue, we have that

$$\begin{aligned} f_i(q) &= \lambda^L(q_i, S_{m,l}(q_{-i})), \\ g_i(q) &= \lambda^C(q_i, S_{m,l}(q_{-i})) + \lambda_{\text{buy}}^M \mathbb{1}_{\text{bestask}(q)=i}, \quad \text{if } i > 0, \\ g_i(q) &= \lambda^C(q_i, S_{m,l}(q_{-i})) + \lambda_{\text{sell}}^M \mathbb{1}_{\text{bestbid}(q)=i}, \quad \text{if } i < 0, \end{aligned}$$

where the function $S_{m,l}(q_{-i})$ is responsible for the interaction between the bid and the ask side of the book, that is,

$$\begin{aligned} S_{m,l}(q_{-i}) &= Q^0 \quad \text{if } q_{-i} = 0, \\ S_{m,l}(q_{-i}) &= Q^- \quad \text{if } 0 < q_{-i} \leq m, \\ S_{m,l}(q_{-i}) &= \bar{Q} \quad \text{if } m < q_{-i} \leq l, \\ S_{m,l}(q_{-i}) &= Q^+ \quad \text{if } q_{-i} > l, \end{aligned}$$

being m and l two fixed thresholds. For example, given a certain volume at the bid side, a new bid limit order has different intensities depending on whether the volume at the ask is, e.g., $q_i = 0$,

$0 < q_i \leq 5$, $5 < q_i \leq 10$ or $q_i > 10$. Market orders may arrive only at the best quote. Moreover, we assume that λ_i^L and λ_i^C are also functions of $\mathbb{1}_{q_{\pm 1} \geq 0}$, for $i \neq \pm 1$, to allow for interactions between the best level and the dynamics far from the best level.

Conditionally on the LOB state, the arrival of different orders at a given limit is assumed to be independent, and follows a Poisson distribution, with intensity equal to λ . However, since the queue sizes depend on the order flow, the model reproduces some auto- and cross-correlations between the components of the order flow, as observed in empirical data.

Contrary to the ZI model, the QR gives a dynamic that is not entirely driven by the orders arriving on the LOB. To achieve this, two additional parameters are introduced, θ and θ^{reinit} . Whenever the mid-price changes, an auxiliary (not observed) price, called the reference price and denoted by p_{ref} , changes in the same direction with probability θ and by an amount equal to the tick size of the asset. Moreover, when p_{ref} changes, the LOB state is redrawn from its invariant distribution around the new value of p_{ref} , with probability θ^{reinit} . In fact, as the authors explain, the parameter θ^{reinit} captures the percentage of price changes due to exogenous information.

In the next subsection we address the procedures that we followed to estimate the two LOB models and discuss the differences between them in terms of ability of reproducing realistic features of empirical high-frequency data.

2.2 Calibration procedures

For the calibration of the ZI and QR models, we used order-book data of the stock Microsoft (MSFT) over the period April 1, 2018 - April 30, 2018. Data were retrieved from the LOBSTER database. Microsoft is a very liquid stock with an average spread approximately equal to 1.25 ticks and thus can be considered a large tick asset, suitable to be modeled by the queue-reactive design.

Before the calibration, for each day we removed from the sample the first hour of trading activity after the market opening and the last 30 minutes before the market closure; this is a standard procedure adopted when working with high-frequency data, since during these two moments of the day the trading activity is known to be more intense and volatile, thereby possibly leading to a violation of the large tick asset hypothesis, even for a liquid stock like Microsoft. Given the average spread observed, and being the activity almost fully concentrated at the best limits, we implemented the ZI and QR models using two limits, $Q_{\pm 1}$ and $Q_{\pm 2}$. This is in line with Huang et al. (2015).

To estimate the intensities of order arrivals under the QR model, the following inputs are needed:

- the type of each event, i.e., limit order, cancel order or market order;
- the time between events that happen at Q_1 and Q_2 , along with the queue sizes q_1 and q_2 before each event;
- the size of each event, as q_i is expressed as a multiple of the median event size.

The estimation of the intensities is performed via maximum likelihood, as in Huang et al. (2015). The parameters m and l that capture the bid-ask dependence are set equal to the the 33% lower

and upper quantiles of the q_{-i} 's (conditional on positive values). Given the symmetry property of the LOB, intensities are computed for just one side.

The parameters θ and θ^{reinit} are calibrated using the mean-reversion ratio ζ of the mid-price, which is defined as

$$\zeta := \frac{n_c}{2n_a},$$

where n_c is the number of continuations (i.e., the number of consecutive price moves in the same directions) and n_a is the number of alternations (i.e., the number of consecutive price moves in opposite directions). For more details about the relation between the mean-reversion ratio and the microstructure of large tick assets, see Robert and Rosenbaum (2011).

We carried out the calibration using a two-step generalized method of moments (GMM), which is more robust than the heuristic approach proposed by Huang et al. (2015). Denote by σ^{emp} and ζ^{emp} the empirical estimates of the standard deviation and mean-reversion ratio of the mid-price returns, computed at the 1-second frequency using the last tick rule. Further, denote by $\sigma_t(\bar{\theta})$ and $\zeta_t(\bar{\theta})$ the quantities estimated in simulation t , with $t = 1, \dots, T$, and $\bar{\theta} = (\theta, \theta^{\text{reinit}})$.

Two-step GMM-based procedure for the calibration of $\bar{\theta}$.

Step 1. Obtain a consistent estimate of $\bar{\theta}$ via the estimator

$$\bar{\theta}_1 := \arg \min_{\bar{\theta} \in [0,1] \times [0,1]} \frac{1}{T^2} \left[\left(\sum_t g_t^\sigma(\bar{\theta}) \right)^2 + \left(\sum_t g_t^\zeta(\bar{\theta}) \right)^2 \right],$$

where $g_t^\sigma(\bar{\theta}) = \frac{\sigma_t(\bar{\theta})}{\sigma^{\text{emp}}} - 1$, $g_t^\zeta(\bar{\theta}) = \frac{\zeta_t(\bar{\theta})}{\zeta^{\text{emp}}} - 1$.

Step 2. Obtain the GMM-estimate of $\bar{\theta}$

$$\theta_{GMM} := \arg \min_{\bar{\theta} \in [0,1] \times [0,1]} \left(\frac{1}{T} \sum_t \bar{g}_t(\bar{\theta}) \right)' W \left(\frac{1}{T} \sum_t \bar{g}_t(\bar{\theta}) \right),$$

where $\bar{g}_t(\bar{\theta}) = (g_t^\sigma(\bar{\theta}), g_t^\zeta(\bar{\theta}))$ and $W^{-1} = \frac{1}{T} \sum_t (\bar{g}_t(\bar{\theta}_1))' (\bar{g}_t(\bar{\theta}_1))$.

The estimator is asymptotically efficient in the GMM class. For the implementation we used $T = 100$ simulations with an horizon of one trading day. The tick size was set equal to the minimum bid-ask spread recorded in the data, namely 1 cent. As a final estimate, we obtained $\theta = 0.6$ and $\theta^{\text{reinit}} = 0.85$.

The asymptotic distribution of the queue size, needed for the re-initialization of the LOB state,

was obtained following the approach proposed by Huang et al. (2015). For each simulated path, the starting LOB state was randomly chosen using the asymptotic distribution of the queue size.

For the calibration of the ZI model, one only needs to reconstruct the intensities of order arrivals. To do that, the only information needed involves the type of order, the order arrival time and the order size. The ensuing estimators read

$$\lambda^L = \frac{\#L}{\#O\overline{\Delta t}}, \quad \lambda^C = \frac{\#C}{\#O\overline{\Delta t}}, \quad \lambda^M = \frac{\#M}{\#O\overline{\Delta t}}$$

where $\#O = \#L + \#C + \#M$ and $\#L$, $\#C$, $\#M$ denote, respectively, the total number of limit, cancel and market orders arriving at the best quotes or between the spread, while $\overline{\Delta t}$ is the average elapsed time between two consecutive orders.

2.3 Comparison of volatility and noise features

As pointed out by Gatheral and Oomen (2010), neither the efficient price nor its volatility are well-defined under the ZI model. The same holds under the QR model. However, if one assumes constant model parameters, thanks to the ergodicity of the processes (see Huang et al. (2015)), the variance of the efficient price can be defined, following Gatheral and Oomen (2010), as

$$\sigma^2 := \lim_{m \rightarrow \infty} \frac{1}{m} E \left[(p(m) - p(0))^2 \right], \quad (1)$$

where p may denote any price process among those considered, that is, the mid-price, the micro-price and the trade price.

Based on (1), given the (calibrated) values of the LOB parameters, it is possible to estimate the true value of σ^2 via simulations. Specifically, in our study, given the LOB parameters calibrated on the Microsoft sample data, numerical results over 2500 simulations show that for $m > 18000$ the volatility of mid-prices, micro-prices and trade-prices stabilizes around the value $\sigma^2 = 1.039 \cdot 10^{-8}$ in the case of the QR model.

Since the knowledge of the value of σ^2 is crucial to compare the finite-sample performance of volatility estimators, we wish to verify whether the two order-book models give similar results. The estimates of σ^2 for the two models and for the three price series considered are compared in Table 1. The levels of variance obtained with the ZI model and the QR are significantly different, even when considering the error in the estimation procedure, with the ZI producing a level about 50% higher than the one observed for the QR model. This highlights a first fact to be considered: the choice of the LOB model is not irrelevant for applications involving the volatility parameter. In fact, it is known that the ZI model calibrated on real data only partially reproduces the actual empirical variance, with a bias which depends on the relative magnitude of the intensities (see, e.g., Bouchaud et al., 2018).

Moreover, since we are interested in comparing the performance of noise-robust volatility esti-

Order-book model	statistics	mid-price	micro-price	trade price
ZI model	Variance	$1.539 \cdot 10^{-8}$	$1.539 \cdot 10^{-8}$	$1.539 \cdot 10^{-8}$
	Std. error	$1.259 \cdot 10^{-9}$	$2.434 \cdot 10^{-9}$	$2.587 \cdot 10^{-9}$
QR model	Variance	$1.039 \cdot 10^{-8}$	$1.039 \cdot 10^{-8}$	$1.039 \cdot 10^{-8}$
	Std. error	$3.336 \cdot 10^{-10}$	$3.330 \cdot 10^{-10}$	$3.319 \cdot 10^{-10}$

Table 1: Comparison of the estimated variance reconstructed via Eq. (1) using simulations of the ZI and the QR models.

mators, we wish to discriminate between the two LOB models on the basis of how well they mimic the noise accumulation observable in empirical data at different frequencies. To do so, we use the Hausman test for the null hypothesis of the absence of noise by Aït-Sahalia and Xiu (2019). In particular, we use the formulation of the test in Equation (16) of Aït-Sahalia and Xiu (2019), which is coherent with the use of LOB models with a constant variance parameter.

Tables 2, 3 and 4 illustrate the frequencies (in seconds) at which the Hausman test rejects the null hypothesis of the absence of noise with a significance level of 5% (★) and the frequencies at which the null is instead not rejected (†) for, respectively, the MSFT sample and the simulated samples from the ZI and QR models. The results of Hausman test suggest that the noise accumulation mechanism at different frequencies under the QR model is more realistic than the one observed under the ZI model, based on the comparison with the noise-detection pattern in the MSFT sample. This aspect is clearly relevant when analyzing the finite-sample performance of noise-robust volatility estimators, and adds empirical support to the use of the QR model for that purpose.

	1 sec.	2 sec.	5 sec.	10 sec.	15 sec.	30 sec.	60 sec.
Mid-price	★	★	★	★	★	†	†
Micro-price	★	★	★	★	★	†	†
Trade-price	★	★	★	★	★	★	†

Table 2: Hausman test results at different frequencies (in seconds) for Microsoft (April 2018). The symbol ★ (†) indicates that the null of absence of noise is rejected (not rejected) with a significance level of 5%.

Lastly, we look at the average spread that the two order-book models are able to generate. This aspect is of paramount importance, being the spread a crucial characteristic of LOB and one of the main sources of market microstructure noise. Table 5 suggests that, even though both the ZI and the QR models generate an average spread lower than the one empirically observed, the underestimation is less severe in the case of the QR. The underestimation of spread under the ZI model has been documented in Bouchaud et al. (2018).

	1 sec.	2 sec.	5 sec.	10 sec.	15 sec.	30 sec.	60 sec.
Mid-price	★	★	★	★	†	†	†
Micro-price	★	★	★	†	†	†	†
Trade-price	★	★	★	†	†	†	†

Table 3: Hausman test results at different frequencies (in seconds) for the ZI model. The symbol ★ (†) indicates that the null of absence of noise is rejected (not rejected) with a significance level of 5%.

	1 sec.	2 sec.	5 sec.	10 sec.	15 sec.	30 sec.	60 sec.
Mid-price	★	★	★	★	★	†	†
Micro-price	★	★	★	★	★	†	†
Trade-price	★	★	★	★	★	†	†

Table 4: Hausman test results at different frequencies (in seconds) for the QR model. The symbol ★ (†) indicates that the null of absence of noise is rejected (not rejected) with a significance level of 5%.

Data	Average spread
MSFT sample	1.25
ZI simulations	1.03
QR simulations	1.14

Table 5: Comparison of the average spread (expressed in ticks) computed from the empirical MSFT sample with the corresponding values obtained from simulations of the ZI and QR samples.

3 Volatility estimators

In this section, we briefly describe the noise-robust integrated- and spot-volatility estimators whose performance will be studied in the next section. The formulae for the tuning parameters involved in the computation of the estimators that optimize the mean squared error (MSE) are also reported.

3.1 Preliminary notation

We consider the estimation horizon $[t, t + h]$, $t, h > 0$, and assume that the price p is sampled on the equally-spaced grid with mesh h/n , where n denotes the number of price observations. The quantity p_i denotes the log-price of the asset at time $t_i := t + ih/n$, $i = 0, 1, \dots, n$. Further, we define $\Delta p_i := p_i - p_{i-1}$. Note that p may refer indifferently to the trade-, mid- or micro-price.

The spot volatility at time t is denoted by $\sigma^2(t)$ and

$$IV_{t,u} := \int_t^{t+u} \sigma^2(s) ds$$

denotes the integrated volatility on $[t, t + u]$, $u \leq h$. Clearly, in a setting with constant volatility $\sigma^2(t) = \sigma^2$ for all t , the latter simplifies to $\sigma^2 u$.

As an auxiliary quantity for the implementation of some estimators, we will need to estimate the integrated quarticity, that is,

$$IQ_{t,u} := \int_t^{t+u} \sigma^4(s) ds.$$

In the rest of the paper, we drop the subscript of both IV and IQ as we always refer to the interval $[t, t + h]$.

Furthermore, we recall that the asymptotic properties of high-frequency volatility estimators are typically derived under the assumption that, for all t , the observable price p is decomposed as

$$p(t) = p^{eff}(t) + \eta(t),$$

where p^{eff} denotes the efficient price, whose dynamics follow an Itô semimartingale, while η is an i.i.d. zero-mean noise due to the market microstructure. As additional auxiliary quantities, we will need estimates of the second moment of η , i.e.,

$$\omega^2 := E[\eta^2]$$

Finally, we denote the floor function as $\lfloor \cdot \rfloor$ and the rounding to the nearest integer as $\lceil \cdot \rceil$.

3.2 Integrated volatility

Bias-corrected realized variance

The realized variance, that is, the sum of squared log-returns over a given time horizon, represents the most natural rate-efficient estimator of the integrated volatility in the absence of noise. However, in the presence of noise, as it is typically the case for high-frequency settings, the realized variance is biased. The bias-corrected realized variance by Zhou (1996) corrects for the bias due to noise by taking into account the first order auto-covariance of the log-returns. The estimator reads:

$$IV_{BC} := c \sum_{j=0}^{q-1} \left(\sum_{i=1}^{c_2} (p_{iq+j} - p_{(i-1)q+j}) \right)^2 + 2 \sum_{i=1}^{c_2-1} (p_{iq+j} - p_{(i-1)q+j})(p_{(i+1)q+j} - p_{iq+j}),$$

where $c = \frac{n}{n-q+1} \frac{1}{q}$ and $c_2 = \lfloor (n-j+1)/q \rfloor$.

The MSE-optimal value of q is attained as

$$q^* = \max \left(1, \left\lfloor \frac{2n\omega^2}{IV\sqrt{3}} \right\rfloor \right).$$

Fourier estimator

Introduced by Malliavin and Mancino (2002, 2009), the Fourier estimator of the integrated volatility relies on the computation of the zero-th Fourier coefficient of the volatility, given the Fourier coefficients of the log-returns. The noise is filtered out by suitably selecting the cutting frequency N . If one uses the Fejér (respectively, Dirichlet) kernel to weight the convolution product, the estimator is defined as

$$IV_F^{Fej} := \frac{(2\pi)^2}{N+1} \sum_{|k| \leq N} \left(1 - \frac{|k|}{N+1} \right) c_k(dp_n) c_{-k}(dp_n),$$

and

$$IV_F^{Dir} := \frac{(2\pi)^2}{2N+1} \sum_{|k| \leq N} c_k(dp_n) c_{-k}(dp_n),$$

where

$$c_k(dp_n) = \frac{1}{2\pi} \sum_{j=1}^n e^{-ikt_j} \Delta p_j$$

represents the k -th discrete Fourier coefficient of the log-return.

The optimal value of the integer N in the presence of noise can be selected by performing a feasible minimization of the MSE, see Mancino and Sanfelici (2008).

In this paper, we implemented IV_F^{Fej} , as unreported simulations suggest that it performs better than IV_F^{Dir} .

Maximum likelihood estimator

The maximum-likelihood estimator by Ait-Sahalia, Mykland, et al. (2005) is based on the assumption that noisy log-returns follow an MA(1) model, consistently with the seminal microstructure model for the bid-ask spread by Roll (1984). Under the MA(1) assumption, it holds that

$$\Delta p_i = w_i + \phi w_{i-1}, \quad (2)$$

and the maximum-likelihood estimator reads

$$IV_{ML} := n \hat{\sigma}_w^2 (1 + \hat{\phi})^2,$$

where the pair $(\hat{\phi}, \hat{\sigma}_w^2)$ is the result of the standard maximum-likelihood estimation of the MA(1) model.

Two-scale estimator

The two-scale realized variance by L. Zhang et al. (2005) eliminates the noise-induced bias of the realized variance by combining two different realized variance values, one computed at a higher frequency and one computed at a lower frequency. The estimator reads:

$$IV_{TS} := c \left(\frac{1}{q} \sum_{j=0}^{q-1} \sum_{i=1}^{\lfloor (n-j+1)/q \rfloor} (p_{iq+j} - p_{(i-1)q+j})^2 - \frac{n-q+1}{nq} \sum_{i=1}^n \Delta p_i^2 \right),$$

where $c = \left(1 - \frac{n-q+1}{nq}\right)^{-1}$. The MSE-optimal value of q is equal to

$$q^* = n^{2/3} \left(\frac{12\omega^4}{IQ} \right)^{1/3}.$$

Multi-scale estimator

L. Zhang (2006) also proposed a more sophisticated combination of realized variances at various frequencies that smooths out the effect of microstructure noise. The multi-scale estimator reads:

$$IV_{MS} := \sum_{j=1}^q \frac{a_j}{j} \sum_{k=0}^{j-1} \sum_{i=1}^{\lfloor (n-k+1)/j \rfloor} (p_{ij+k} - p_{(i-1)j+k})^2,$$

where

$$a_j = j(1 - 1/q^2)^{-1} \left(\frac{12(1/q - 1/2)}{q^2} - \frac{6}{q^3} \right).$$

The MSE-optimal q is given by

$$q^* = \sqrt{n} \left(\beta + \sqrt{\beta^2 + \frac{144\omega^4}{104/35IQ}} \right)^{1/2},$$

where $\beta = \frac{48/5\omega^2(IV + \omega^2/2)}{208/35IQ}$.

Kernel estimator

Kernel-based estimators, originally introduced by Barndorff-Nielsen et al. (2008), correct for the bias due to noise of the realized variance by taking into account the autocorrelation of returns at different lags, suitably weighted by means of a kernel function $k(\cdot)$. The estimator reads:

$$IV_K := \sum_{i=1}^n \Delta p_i^2 + 2 \sum_{j=1}^q k\left(\frac{j-1}{q}\right) \sum_{i=1}^{n-j} \Delta p_i \Delta p_{i+j}.$$

Moreover, the MSE-optimal value of q is equal to

$$q^* = \sqrt{n} \left(\beta + \sqrt{\beta^2 + \frac{c\omega^4}{aIQ}} \right)^{1/2},$$

where $\beta = \frac{b\omega^2(IV + \omega^2/2)}{2aIQ}$, $a = 4 \int_0^1 k(x)^2 dx$, $b = -8 \int_0^1 k(x)k''(x)dx$, $c = 12(k'''(0) + \int_0^1 k(x)k'''(x)dx)$.

In this paper we implemented this estimator by using the Tukey Hanning 2 kernel, i.e., we set $k(x) = \sin^2(\pi/2(1-x)^2)$. This kernel was shown to perform satisfactorily, compared to other kernels (see Barndorff-Nielsen et al. (2008)).

Pre-averaging estimator

The pre-averaging estimator, proposed by Jacod et al. (2009), relies on the averaging of the price values over a window h to compute the realized variance, together with a bias-correction term. The estimator is as follows:

$$IV_{PA} := \frac{6}{h} \sum_{s=0}^{n-h+1} \left(\frac{1}{h/2} \sum_{s'=0}^{h/2-1} p_{s+s'+h/2} - \frac{1}{h/2} \sum_{s'=0}^{h/2-1} p_{s+s'} \right)^2 - \frac{6}{h^2} \sum_{i=1}^n \Delta p_i^2.$$

Jacod et al. (2009) suggest that the estimator is robust to the choice of h ; in our simulation study we set h to obtain a window of approximately 4 minutes, in line with Y. Li, Liu, et al. (2021).

Alternation estimator

Proposed by Large (2011), the alternation estimator corrects the realized variance with a factor dependent on the number of alternations and continuations in the sample, that is, the estimator reads

$$IV_{Alt} := \frac{n_c}{n_a} \sum_{i=1}^n \Delta p_i^2,$$

where n_c is the number of consecutive price movements in the same direction, while n_a the number of consecutive price movement in the opposite direction.

MinRV and MedRV estimators

Andersen et al. (2012) introduced two jump-robust estimators of the integrated variance which consist, respectively, in the (scaled) sum of the minimum or the median between consecutive returns, that is,

$$IV_{Min} = \frac{\pi}{\pi - 2} \left(\frac{n}{n-1} \right) \sum_{i=1}^{n-1} \min(|\Delta p_i|, |\Delta p_{i+1}|)^2;$$
$$IV_{Med} = \frac{\pi}{6 - 4\sqrt{3} + \pi} \left(\frac{n}{n-2} \right) \sum_{i=2}^{n-1} \text{med}(|\Delta p_{i-1}|, |\Delta p_i|, |\Delta p_{i+1}|)^2.$$

To make the estimators robust to the presence of microstructure noise, pre-averaging may be applied to price observations, as shown in Andersen et al. (2012), Appendix B. Accordingly, in this paper we used the noise-robust version of IV_{Min} and IV_{Med} with price pre-averaging.

Range estimator

The main idea behind the range estimator by Vortelinos (2014) is to substitute the simple returns with the difference between the maximum and minimum observed price over a given window, to obtain the estimator

$$IV_{RG} := \frac{1}{4 \log(2)} \sum_{i=1}^{n/q} (max_{qi} - min_{qi})^2,$$

where $max_{qi} = \max(p_{(i-1)q}, \dots, p_{iq})$ and $min_{qi} = \min(p_{(i-1)q}, \dots, p_{iq})$. The MSE-optimal frequency is

$$q^* = \left(\frac{IQ}{\omega^4} \right)^{1/3}.$$

Unified estimator

Y. Li, Z. Zhang, et al. (2018) proposed a unified approach to volatility estimation, obtaining an estimator which is consistent not only in the presence of the typical i.i.d. noise, but also when the noise comes from price rounding. The estimator is defined as follows:

$$IV_U := \sum_{l=1}^m \left(\frac{1}{m} - \bar{n} \frac{n_l - \bar{n}}{\sum_{j=1}^L n_j^2 - h\bar{n}^2} \right) \frac{1}{q_l} \sum_{k=0}^{q_l-1} \sum_{i=1}^{n_l} (p_{(k+i)q_l} - p_{k+(i-1)q_l})^2,$$

where $\bar{n} = (\sum_{l=1}^m n_l)/h$, $n_l = n/q_l$ and $q_{l+1} = q_l + l$, $l = 1, \dots, m-1$. The optimal q_1 and h can be selected via the data-driven procedure detailed in Y. Li, Z. Zhang, et al. (2018).

3.3 Spot volatility

Fourier estimator

The Fourier method allows reconstructing the trajectory of the volatility as a function of time on a discrete grid, see Mancino and Recchioni (2015). This is achieved by means of the Fourier-Fejér inversion formula, which gives the estimator

$$\sigma_F^2(t) := \sum_{|k| \leq M} \left(1 - \frac{|k|}{M+1} \right) e^{itk} c_k(\sigma_{n,N}^2), \quad t \in [0, 2\pi],$$

where

$$c_k(\sigma_{n,N}^2) = \frac{2\pi}{2N+1} \sum_{|s| \leq N} c_s(dp_n) c_{k-s}(dp_n)$$

estimates the k -th Fourier coefficient of the volatility. Note that, differently from the other estimators detailed below, the Fourier estimator is *global*, in the sense that it estimates the entire volatility function on a discrete grid over the interval $[0, 2\pi]^1$, instead of a local value at a specific time t .

The efficient selection of N and M can be performed based on the numerical results given Mancino and Recchioni (2015).

Regularized estimator

Proposed by Ogawa (2008), the regularized estimator is based on a regularization procedure that involves data around the estimation point. The estimator reads

$$\sigma_{REG}^2(t) := \frac{3s^2}{q\sqrt{[n/q]}(3sq - q^2 + 1)} \sum_{i=1}^{[n/q]} \Delta \bar{p}_{t+i}^2,$$

¹By suitably re-scaling the unit of time, the estimator can be applied to any arbitrary interval.

where

$$\bar{p}_t = \frac{1}{s} \sum_{j=1}^s p_{tq-j+1}.$$

Following Ogawa and Sanfelici (2011), for the implementation we set $q = [n/n_t]$ and $s = 2q$, where n_t is the number of points on which the spot variance trajectory is reconstructed.

Kernel estimator

Fan and Wang (2008) (see also Kristensen (2010)) proposed an estimator of the spot variance based on the localization of the kernel-weighted realized variance over a window of length q , which reads

$$\sigma_K^2(t) := \frac{1}{q} \sum_{t_i=t-q}^{t+q} k\left(\frac{t_i-t}{q}\right) \Delta p_i^2,$$

with

$$q = [\sqrt{n}/\log n].$$

For the implementation, we used the Fejér kernel, following Mancini et al. (2015).

Pre-averaging estimator

The pre-averaging estimator of the spot volatility by Jing et al. (2014) and Y. Li, Liu, et al. (2021) relies on the localization of the pre-averaging integrated estimator on a window of length h and reads

$$\sigma_{PA}^2(t) := \frac{n}{q} \frac{12}{s} \sum_{j=0}^{q-s+1} \frac{1}{2} \left(\frac{1}{s/2} \sum_{j'=0}^{s/2-1} p_{t+j+j'+s/2} - \frac{1}{s/2} \sum_{j'=0}^{s/2-1} p_{t+j+j'} \right)^2 - \frac{n}{q} \frac{6}{s} \sum_{j=0}^q \Delta p_{t+j}^2,$$

with $q = [c_1 n^{3/4}]$ and $s = [c_2 n^{1/2}]$.

The constants c_1 and c_2 can be chosen based on the numerical results in Y. Li, Liu, et al. (2021).

Two-scale estimator

The localized two-scale estimator, proposed by Zu and Boswijk (2014), reads

$$\sigma_{TS}^2(t) := \frac{1}{s} \sum_{j=q}^n \frac{(p_j - p_{j-q})^2}{q} - \frac{\bar{n}}{n} \frac{1}{s} \sum_{j=1}^n \Delta p_j^2,$$

where $\bar{n} = \frac{ns-q+1}{qs}$. The MSE-optimal values of s and q are given by

$$q^* = q^0 n^{2/3} \quad s^* = s^0 n^{-1/6},$$

where

$$q^0 = \left(\frac{12\omega^4}{IQ} \right)^{1/3}$$

and

$$s^0 = \left(\frac{8\omega^4/(q^0)^2 + \frac{4}{3}q^0IQ}{\frac{1}{3}\gamma} \right)^{1/2},$$

with

$$\gamma = \sum_{i=1}^{n-1} (\Delta\sigma^2(t_i))^2, \quad \sigma^2(t_i) = \frac{1}{s} \sum_{j=0}^{s-1} \Delta p_{i+j}^2.$$

Optimal candlestick estimator

The optimal candlestick estimator proposed by J. Li et al. (2022) relies on candlestick data, i.e., the opening, closing, highest and lowest prices within a given interval. Formally, denote by $I_{n,i} := \{(i-1)\Delta_n, i\Delta_n\}$ the interval associated with the i th candlestick, where $\Delta_n \rightarrow 0$ as $n \rightarrow \infty$. Moreover, let O_i, C_i, H_i and L_i denote, respectively, the opening, closing, highest and lowest prices on $I_{n,i}$. The estimator reads

$$\sigma_{OK}^2(t) = \frac{(\lambda_1|O_i - C_i| + \lambda_2(H_i - L_i))^2}{\Delta_n}, \quad t \in I_{n,i}$$

where λ_1 and λ_2 are constants. For the implementation, we set $\Delta_n = 1$ minute (see Section 4) and selected (λ_1, λ_2) based on the optimality conditions detailed in J. Li et al. (2022), Section 2.2.

Pre-averaging kernel estimator

Figueroa-López and Wu (2022) proposed an estimator of the spot variance which consists in a localization of the realized kernel estimator with pre-averaging, i.e.,

$$\sigma_{PAK}^2(t) := \frac{1}{f(g)} \sum_{j=1}^{n-s+1} \frac{1}{q} k\left(\frac{t_{j-1} - t}{q}\right) \left(\bar{p}_j^2 - \frac{1}{2}\hat{p}_j\right)$$

where:

$$\bar{p}_j = - \sum_{i=1}^s \left(g\left(\frac{i}{s}\right) - g\left(\frac{i-1}{s}\right) \right) p_{i+j-2},$$

$$\hat{p}_j = \sum_{i=1}^s \left(g\left(\frac{i}{s}\right) - g\left(\frac{i-1}{s}\right) \right)^2 \Delta p_{i+j-1}^2,$$

$$f(g) = \sum_{i=1}^s g\left(\frac{i}{s}\right)^2,$$

with $g(x) = \min(x, 1-x)$, $q = c_m(h/n)^{1/4}$ and $s = \lfloor 1/(c_k \sqrt{h/n}) \rfloor$.

The authors suggest to use the exponential kernel, that is, $k(x) = \frac{1}{2} \exp(-|x|)$, as it is proved to be the optimal kernel in terms of the minimization of the asymptotic variance (see Figueroa-López and C. Li (2020)). Further, we choose c_k and c_m in accordance with the formulas derived by the authors to optimize the integrated asymptotic variance (see also Remark 4.1 in Figueroa-López and Wu (2022)).

3.4 Feasible selection of tuning parameters

The feasible implementation of the optimization formulae for the tuning parameters which appear in the previous section may require the estimation of IV , IQ and ω^2 . In this regard, we use the following estimators, as in Gatheral and Oomen (2010):

$$\widehat{IV} = \frac{n}{n-q+1} \frac{1}{q} \sum_{s=0}^{q-1} \sum_{i=1}^{\lfloor (n-s+1)/q \rfloor} (p_{iq+s} - p_{(i-1)q+s})^2$$

$$\widehat{IQ} = \left(\frac{n}{n-q+1} \right)^2 \frac{26}{q} \sum_{s=0}^{q-1} \sum_{i=1}^{\lfloor (n-s+1)/q \rfloor} (p_{iq+s} - p_{(i-1)q+s})^4$$

$$\hat{\omega}^2 = -\hat{\phi} \hat{\sigma}_w^2, \quad \hat{\omega}^4 = (\hat{\omega}^2)^2,$$

where the pair $(\hat{\sigma}_w^2, \hat{\phi})$ is obtained as in (2).

Note that q is selected in correspondence of the 5-minute (noise-free) sampling frequency.

4 Comparative performance study of volatility estimators

In this section we present the results of a study of the finite-sample performance of the volatility estimators described in the previous section, which is based on simulations of the QR model. In the study, we considered two alternative scenarios. In the first scenario, we assumed constant values of the parameters θ and θ^{reinit} , which translate into a constant volatility parameter. Instead, in the second scenario we allowed θ and θ^{reinit} to change, so that the volatility parameter is no longer constant. We emphasize the fact that this second scenario introduces a novelty compared to the study by Gatheral and Oomen (2010), where the volatility parameter is constant. In fact, a scenario with time-varying volatility offers a more realistic framework to assess the performance of estimators.

For each scenario, we simulated 2500 daily paths. For each couple $(\theta, \theta^{reinit})$ considered, the corresponding true value of the volatility parameter was obtained via additional simulations exploiting Eq. (1), as described in Subsection 2.3. Estimators were computed using 1-second price observations. The integrated volatility was estimated on daily intervals, while for the spot volatility we reconstructed daily trajectories on the 1-minute grid. The selection of the tuning parameters involved in the computation of the different estimators was performed based on the feasible formulae and the suggestions reported in the previous section.

4.1 Constant θ and θ^{reinit}

In the first scenario, simulations were performed with θ and θ^{reinit} constant and equal to, respectively, 0.6 and 0.85, that is, the parameter values calibrated on the MSFT sample (see Section 2). We recall that the resulting reference value of the spot variance parameter is $\sigma^2 = 1.0387 \cdot 10^{-8}$ (see Subsection 2.3).

Tables 6-9 display the ranking of the estimators for the three series of mid-price, micro-price and trade-price in terms of their finite-sample performance. The latter is evaluated by means of, resp., the relative bias and MSE for the integrated volatility and the relative integrated bias and MSE for the spot volatility. In each table, the estimators are ordered based on the average ranking, obtained as the arithmetic mean of the rankings for the three prices series.

For what concerns integrated estimators, the pre-averaging estimator and the Fourier estimator provide the relative best performance in terms, resp., of bias and MSE minimization, based on the average ranking. However, note that the Fourier estimator achieves the best MSE average ranking without resulting the first in the ranking for any price series. Indeed, the unified volatility estimator, which is robust to i.i.d. noise and rounding, yields the best performance for mid- and micro-prices, while the best result for trade-prices is achieved by the alternation estimator, which is robust to price discreteness and rounding (see Large (2011)). Overall, this may suggest that robustness to rounding may be crucial to optimize the mean squared error. Instead, the pre-averaging estimator is more clearly favorable in terms of bias reduction, given the fact that it results the first in terms of bias minimization for micro- and trade-price series and the second for mid-price series. Moreover, it is worth noticing that the Min RV and Med RV, which are also computed from pre-averaged data, occupy the second and third places in the average ranking for the bias.

As for spot estimators, simulations indicate that the Fourier estimator outperforms the other estimators considered, both in terms of bias and MSE optimization, for all the price series considered. Only the regularized estimator is capable of obtaining comparable performances in terms of bias. The Fourier estimator differs from the other spot estimators considered in that it relies on the integration of the Fourier coefficients of the volatility rather than on the differentiation of the (estimated) integrated variance, and this appears to represent a solid numerical advantage. Figure 1 shows sample trajectories of the spot estimators computed from the mid-price series, along with the true volatility value, to help better understand the difference in performance among the estimators. Appendix A.2 contains the analogous figures for the micro-price and the trade-price.

Finally, in the case of both integrated and spot estimators we investigated whether the volatility values obtained using different methods were statistically different. To this end, for each pair of estimators, we performed a t-test of the null hypothesis that the mean value of the estimated volatility is the same. As a result, we found that all average estimations are pairwise significantly different at the 1% confidence level. Moreover, to better assess the differences in the performances of estimators, we also applied the model confidence set (MCS) procedure by Hansen, Lunde, and Nason (2011), with a significance level of 1%. Following Patton (2011), for the MCS we used the

qlike loss function. As a result, the MCS procedure always chooses as the optimal model set the one containing only the estimator with the best ranking in terms of MSE (see Tables 7 and 9), thus supporting the soundness of our results. Overall, the results of the t-tests and the MCS offer additional support to the fact that the careful selection of the estimation method is not irrelevant.

Integrated variance estimators - relative bias							
Estimator	mid-price	rank	micro-price	rank	trade-price	rank	av. rank
Pre-averaging	-0.01106	2	-0.00643	1	-0.00534	1	1.33
Min RV	0.01071	1	0.01050	2	0.01181	3	2
Med RV	0.01367	3	0.01348	3	0.01456	4	3.33
Unified	0.05518	4	0.04679	4	0.11442	7	5
Fourier	0.09154	6	0.08290	5	0.09234	6	5.66
Range	-0.09196	7	-0.08302	6	-0.06997	5	6
Alternation	0.06799	5	0.11612	12	-0.06226	2	6.33
Kernel	0.12679	8	0.10075	8	0.24836	8	8
Maximum likelihood	0.13990	12	0.10011	7	0.27243	9	9.33
Two-scale RV	0.12827	9	0.10465	9	0.32015	10	9.66
Multi-scale RV	0.12841	10	0.10478	10	0.32030	11	10.33
Bias-corrected RV	0.12852	11	0.10489	11	0.32042	12	11.33

Table 6: Performance and ranking of the integrated variance estimators for the series of mid-price, micro-price and trade-price, according to the relative bias. The average ranking is reported in the last column.

Integrated variance estimators - relative MSE							
Estimator	mid-price	rank	micro-price	rank	trade-price	rank	av. rank
Fourier	0.00981	3	0.00658	2	0.01039	2	2.33
Unified	0.00433	1	0.00346	1	0.01446	6	2.66
Alternation	0.00593	2	0.01145	5	0.00485	1	2.66
Med RV	0.01075	4	0.01174	6	0.01181	3	4.33
Min RV	0.01275	5	0.012754	7	0.01282	4	5.33
Maximum likelihood	0.01647	7	0.01112	3	0.07564	9	6.33
Kernel	0.01726	9	0.01128	4	0.06314	8	7
Pre-averaging	0.01566	6	0.015653	11	0.01568	7	8
Multi-scale RV	0.01648	8	0.012070	8	0.10401	11	9
Range	0.01794	12	0.016448	12	0.01304	5	9.66
Two-scale RV	0.01757	10	0.012901	10	0.10391	10	10
Bias-corrected RV	0.01734	11	0.012094	9	0.10409	12	10.66

Table 7: Performance and ranking of the integrated variance estimators for the series of mid-price, micro-price and trade-price, according to the relative mean squared error. The average ranking is reported in the last column.

Spot variance estimators - relative integrated bias							
Estimator	mid-price	rank	micro-price	rank	trade-price	rank	av. rank
Fourier	0.00362	1	0.00299	1	0.00713	1	1
Regularized	0.00676	2	0.00663	2	0.00802	2	2
Optimal candlestick	-0.16165	3	-0.12525	3	-0.07430	3	3
Pre-averaging kernel	-0.14755	4	-0.13462	4	-0.08459	4	4
Pre-averaging	0.19939	5	0.19923	5	0.19936	6	5.33
Kernel	0.22205	6	0.23801	6	0.73200	7	6.33
Two-scale	-0.24781	7	-0.26271	7	-0.11798	5	6.33

Table 8: Performance and ranking of the spot variance estimators for the series of mid-price, micro-price and trade-price, according to the relative integrated bias. The average ranking is reported in the last column.

Spot variance estimators - relative integrated MSE							
Estimator	mid-price	rank	micro-price	rank	trade-price	rank	av. rank
Fourier	0.03095	1	0.03060	1	0.03128	1	1
Pre-averaging kernel	0.13392	2	0.13745	2	0.09148	2	2
Regularized	0.20632	3	0.20628	3	0.20635	3	3
Optimal candlestick	0.31790	4	0.31436	4	0.33429	4	4
Kernel	0.46111	5	0.47095	5	0.84365	5	5
Two-scale	1.62190	6	1.59843	6	2.24599	6	6
Pre-averaging	2.59134	7	2.59064	7	2.59247	6	7

Table 9: Performance and ranking of the spot variance estimators for the series of mid-price, micro-price and trade-price, according to the relative integrated mean squared error. The average ranking is reported in the last column.

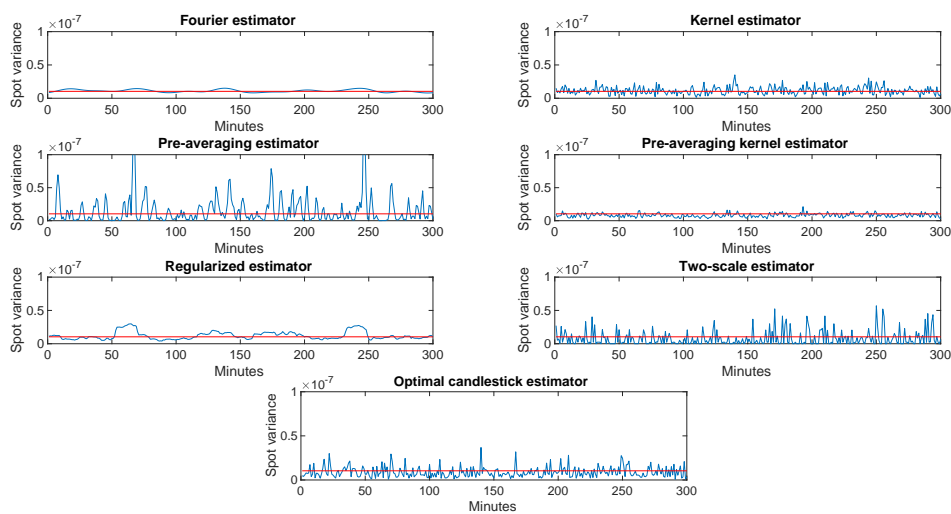


Figure 1: Constant θ and θ^{reinit} : sample trajectories of spot variance estimators computed from mid-prices (in blue) and true volatility (in red).

4.2 Variable θ and θ^{reinit}

A nice feature of the QR model, compared to the ZI model, is the flexibility introduced by the parameters θ and θ^{reinit} . In the second scenario we assessed the effect of time-varying values of θ and θ^{reinit} on the accuracy of volatility estimators. Specifically, we allowed for piece-wise constant volatility dynamics, which might describe a regime-shifting scenario driven, for example, by the flow of information hitting the market.

We considered two sub-scenarios, with increasing variability of the volatility parameter. In the first one, the LOB follows five regimes (each with length equal to 1/5 of a day), which translate into a double u-shaped pattern for the volatility parameter, as illustrated in Table 10.

Period	θ	θ^{reinit}	σ^2
I	0.7	0.6	$1.473 \cdot 10^{-8}$
II	0.4	0.6	$8.553 \cdot 10^{-9}$
III	0.6	0.85	$1.039 \cdot 10^{-8}$
IV	0.4	0.9	$7.195 \cdot 10^{-9}$
V	0.8	0.9	$1.366 \cdot 10^{-8}$

Table 10: θ and θ^{reinit} values used for the simulations with five regimes and the corresponding values of σ^2 .

In the second sub-scenario, we allowed for ten regimes (each with length equal to 1/10 of a day), which recreate a u-shape pattern for the volatility parameter, see Table 11.

Period	θ	θ^{reinit}	σ^2	Period	θ	θ^{reinit}	σ^2
I	0.7	0.6	$1.473 \cdot 10^{-8}$	VI	0.3	0.5	$4.813 \cdot 10^{-9}$
II	0.8	0.9	$1.366 \cdot 10^{-8}$	VII	0.4	0.9	$7.195 \cdot 10^{-9}$
III	0.8	0.7	$1.281 \cdot 10^{-8}$	VIII	0.4	0.6	$8.553 \cdot 10^{-9}$
IV	0.5	0.5	$7.753 \cdot 10^{-9}$	IX	0.6	0.85	$1.039 \cdot 10^{-8}$
V	0.2	0.8	$3.068 \cdot 10^{-9}$	X	0.9	0.4	$1.469 \cdot 10^{-8}$

Table 11: θ and θ^{reinit} values used for the simulations with ten regimes and the corresponding values of σ^2 .

Tables 12 and 13 illustrate the average performance rankings in the second scenario. Specifically, average rankings in correspondence of five and ten intra-day regimes are compared with the case of a unique regime (i.e., the case with constant θ and θ^{reinit} illustrated in the previous subsection). Full performance results in terms of bias and MSE are detailed in Appendix A.1.

Overall, it appears that the introduction of time-varying parameters does not significantly affect

the performance rankings previously obtained with constant parameters. In other words, most of the rankings are quite stable (with a few exceptions, see, e.g., the average ranking for the MSE of the Range and Pre-averaging estimators), compared to the first scenario. The stability is more evident for spot variance estimators.

As a further investigation, it might be interesting to study whether the performance ranking remains similar also when the volatility path has infinite regimes, for example when the evolution of θ and θ^{reinit} is driven by stochastic differential equations. This would require to build a precise mapping between the volatility and θ and θ^{reinit} in order to simulate the LOB for each value of the simulated volatility. This interesting investigation is beyond the scope of this paper and is left for future research.

As in the previous subsection, to help better understand the difference in performance among the estimators in the second scenario, Figures 2 and 3 contain sample trajectories of the spot variance estimators computed from mid-price observations, together with the path of the true variance parameter; the analogous figures for micro- and trade-prices are in Appendix A.2.

Average rankings for different volatility regimes (integrated variance)						
Estimator	relative bias			relative MSE		
	1 regime	5 regimes	10 regimes	1 regime	5 regimes	10 regimes
Pre-averaging	1.33	1	2	8	4	4.33
Fourier	5.66	6.33	6.33	2.33	3	3.33
Med RV	3.33	2	1	4.33	5.33	6.66
Min RV	2	3	3.33	5.33	7	8.66
Unified	5	6	5.66	2.66	3	3.33
Range	6	4	5	9.66	3	3.33
Alternation	6.33	7.66	6.33	2.66	5	4.33
Maximum likelihood	9.33	8.66	8	6.33	7.66	6.33
Kernel	8	8.33	9	7	8	8
Two-scale RV	9.66	9.33	9.33	10	9.66	9.66
Multi-scale RV	10.33	10.33	10.66	9	10.66	9
Bias-corrected RV	11.33	11.66	11.66	10.66	11.66	11

Table 12: Average rankings of integrated variance estimators for an increasing number of intra-day volatility regimes.

Average rankings for different volatility regimes (spot variance)						
Estimator	relative int. bias			relative int. MSE		
	1 regime	5 regimes	10 regimes	1 regime	5 regimes	10 regimes
Fourier	1	1	1	1	1	1
Regularized	2	2	2	3	3	3
Pre-averaging kernel	4	3	3	2	2	2
Optimal candlestick	3	4	4.33	4	4	4
Kernel	6.33	6	5.66	5	5	5
Pre-averaging	5.33	5	5.66	7	7	6.66
Two-scale	6.33	7	7	6	6	6.33

Table 13: Average rankings of spot variance estimators for an increasing number of intra-day volatility regimes.

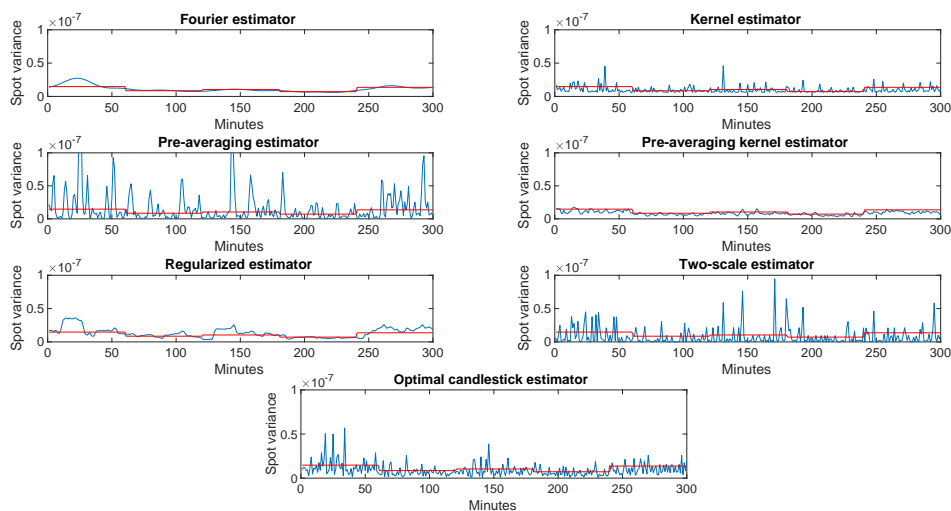


Figure 2: Variable θ and θ^{reinit} (5 regimes): sample trajectories of spot variance estimators computed from mid-prices (in blue) and true volatility (in red).

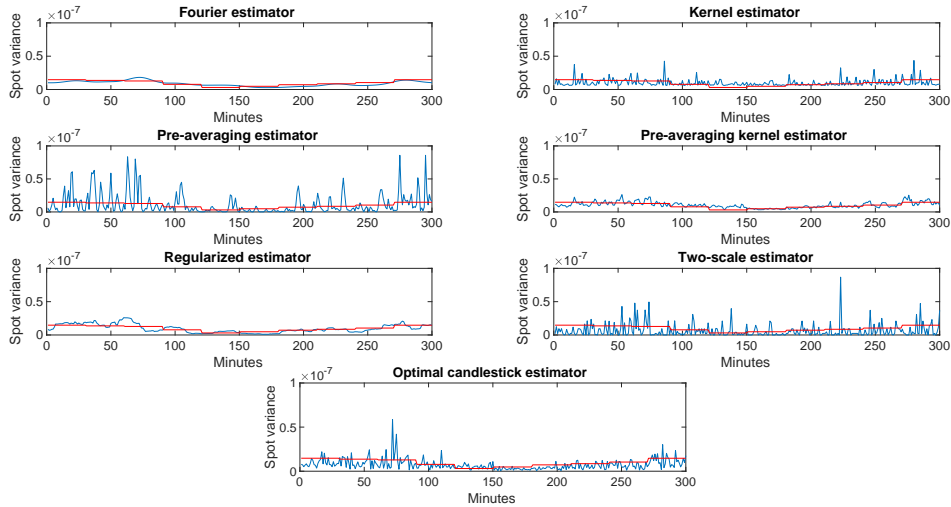


Figure 3: Variable θ and θ^{reinit} (10 regimes): sample trajectories of spot variance estimators computed from mid-prices (in blue) and true volatility (in red).

5 The impact of efficient volatility estimates on optimal execution

In this section, we discuss the results of a study which aims at providing insights into the impact of the use of efficient volatility estimates on the prediction of the variance of the cost of a VWAP execution.

Consider the following problem. A trader has S shares to buy within the interval $[0, T]$. The interval is divided into N_τ time periods of length $\tau = T/N_\tau$ and v_k , $k = 1, \dots, N_\tau$, denotes the (signed) number of shares to be traded in interval k . Clearly, $\sum_{k=1}^{N_\tau} v_k = S$. Moreover, let \tilde{p}_k be the price at which the investor trades in interval k (in general different from the average price in the interval, p_k) and p_0 the price before the start of the execution. The objective function is the *Implementation Shortfall* (IS), defined as

$$C(\mathbf{v}) \equiv \sum_{k=1}^{N_\tau} v_k \tilde{p}_k - S p_0 \quad (3)$$

i.e., as the difference between the cost and the cost in an infinitely liquid market. The IS is in general a stochastic variable, therefore one often wishes to minimize

$$\mathbb{E}[C(\mathbf{v})] + \lambda \text{Var}[C(\mathbf{v})]$$

where λ measures the risk aversion of the trader.

Let us consider a traders which models market impact according to the Almgren and Chriss model (Almgren and Chriss (2001)). In this model, the price of the stock at step k is equal to the previous price plus a linear permanent market impact term and a random shock, that is,

$$p_k = p_{k-1} + \vartheta v_k + u_k \quad u_k \sim \text{IID}(0, \sigma^2 \tau), \quad (4)$$

where σ^2 is instantaneous volatility of the unaffected price. Moreover, the actual price paid \tilde{p}_k is different from the average price p_k in the interval and reads

$$\tilde{p}_k = p_k + \rho v_k, \quad (5)$$

where ρv_k represents a linear temporary impact.

The expected cost of an execution is then given by

$$E[C(\mathbf{v})] = (\vartheta + \rho) \sum_{k=1}^{N_\tau} v_k^2 + \vartheta \sum_{i>j} v_i v_j$$

and its variance is equal to

$$\text{Var}[C(\mathbf{v})] = \sigma^2 \tau \mathbf{v}^T B \mathbf{v},$$

where

$$B = \begin{pmatrix} 1 & 1 & 1 & 1 & \dots \\ 1 & 2 & 2 & 2 & \dots \\ 1 & 2 & 3 & 3 & \dots \\ 1 & 2 & 3 & 4 & \dots \\ \dots & \dots & \dots & \dots & \dots \end{pmatrix}.$$

Note that the variance does not depend on the impact parameters ρ and θ , but only on the volatility. Further, note that the above expression is more general, as it remains valid also when the temporary impact is nonlinear, see Guéant (2016) for more details.

For the sake of simplicity we assume that the trader performs a VWAP execution (i.e., $\mathbf{v} = \frac{S}{N_\tau} (1, 1, \dots, 1)^T$), so that the variance of the cost is equal to

$$\text{Var}[C_{VWAP}] = \frac{\sigma^2 S^2}{N_\tau^2} \tau \sum_{k=0}^{N_\tau-1} (2k+1)(N_\tau - k) = S^2 \sigma^2 \tau \frac{1}{6N_\tau} (2N_\tau^2 + 3N_\tau + 1) \quad (6)$$

This expression shows that, in order to estimate the variance of the execution cost, the traders must have a reliable estimation of σ . We investigate whether the availability of an efficient estimate of the latent volatility parameter could allow the trader to reliably infer the variance of the cost of the

strategy. More specifically, we are interested in assessing whether the use of a specific spot volatility estimator, among those studied in Section 4, leads to a gain in the accuracy of such inference.

To this aim, we use Monte Carlo scenarios of the QR model to simulate a VWAP execution and we compare the variance of the cost of the simulated executions with the corresponding value predicted by the Almgren and Chriss model (see Eq. (6)), evaluated with the (average) value of σ^2 obtained through a specific estimator. Since it is not obvious that the Almgren-Chriss model faithfully describes the market impact in the QR model, we opted for a more robust comparison that considers the ratio of the aforementioned quantities in correspondence of two different values of the couple $(\theta, \theta^{reinit})$, i.e. of the volatility. In this way, the effect of the strategy parameters S, τ and N_τ in equation 3, that depend on the specific market-impact model, disappear.

For the simulation of the execution strategy, we set $T = 3$ hours and 20 minutes, $\tau = 10$ minutes and $S = 60$, so that $N_\tau = 20$ and $\mathbf{v} = (3, \dots, 3)^T$. The strategy was simulated on top of QR dynamics simulated in two different scenarios with parameters $(\theta, \theta^{reinit})$ equal to $(0.6, 0.85)$ and $(0.4, 0.6)$. We considered 100 VWAP executions and we computed the empirical variance of their execution cost. The average spot variance values were retrieved from the study of Section 4.

Table 14 compares the ratios obtained for each spot variance estimator with the benchmark ratio, that is, the ratio of empirical variance costs. Values related to $(\theta, \theta^{reinit}) = (0.6, 0.85)$ (respectively, $(\theta, \theta^{reinit}) = (0.4, 0.6)$) were used at the numerator (respectively, denominator).

Ratios of variances of the VWAP execution cost	
Empirical variance	1.397
Fourier	1.235
Regularized	1.234
Pre-averaging kernel	1.563
Optimal candlestick	1.566
Pre-averaging	1.208
Kernel	1.186
Two-scale	1.030

Table 14: Ratios of variances of the VWAP implementation shortfall in correspondence of, respectively, $(\theta, \theta^{reinit}) = (0.6, 0.85)$ (numerator) and $(\theta, \theta^{reinit}) = (0.4, 0.6)$ (denominator).

Results in Table 14 suggest that the Fourier estimator and the regularized estimator produce the relative best forecasts of the variance of the strategy costs, as they are associated to a ratio approximately equal to 1.23, which is the closest to the benchmark value of 1.397. As these two estimators provide also the relative best performance in terms of bias and MSE (see Section 4), our study suggests that efficient volatility estimates may be linked to a better forecast of the variance of the execution cost. Furthermore, note that the range of variation of the ratios in Table 14 suggests

that the the choice of the estimator is not irrelevant and may lead to significant differences in the forecast of the execution strategy. It seems however that, in general, the use of the formula in Eq. (6) leads to a certain underestimation of the the variance of the implementation shortfall of the considered strategy.

6 Conclusions

This paper extended the work by Gatheral and Oomen (2010) on volatility estimation with LOB data in two directions. First, we used a more sophisticated LOB simulator compared to the ZI model, namely the QR model, which, by introducing correlations between the current state of the LOB and the intensities of order arrival, and thanks to a more complex re-initialization mechanism, is able to produce more realistic market microstructure dynamics.

Secondly, we addressed not only integrated volatility estimators, but also spot volatility estimators. For what concerns integrated estimators, we found that the pre-averaging estimator by Jacod et al. (2009) appears to be favorable in terms of bias optimization. Instead, when looking at the minimization of the MSE, the situation is more nuanced, with the Fourier estimator by Malliavin and Mancino (2009) obtaining the best average ranking across the three different price series considered without actually achieving the best ranking for any of the individual series. Specifically, the MSE is optimized by the unified estimator by Y. Li, Z. Zhang, et al. (2018) (in the case of mid- and micro-prices) and the alternation estimator by Large (2011) (in the case of trade-prices). As for the spot volatility, the Fourier estimator appeared to yield the optimal accuracy both in terms of bias and MSE, outperforming the other estimators considered.

Finally, our results suggested that the careful choice of the spot volatility estimator may be relevant for optimal execution. Specifically, we investigated the impact of different spot volatility estimators on the prediction of the variance of the cost of a VWAP strategy and found that the use of the Fourier estimator, which gave the relative most accurate volatility estimates, lead also to a significant gain in predicting the cost variance.

Acknowledgments

The authors are thankful to Jim Gatheral and Mathieu Rosenbaum for the useful discussions and to Othmane Mounjid for the valuable insights into the implementation of the Queue-Reactive model.

References

Abergel, Frédéric, Marouane Anane, Anirban Chakraborti, Aymen Jedidi, and Ioane Muni Toke (2016). *Limit order books*. Cambridge University Press.

- Aït-Sahalia, Yacine and Jean Jacod (2014). *High-frequency financial econometrics*. Princeton University Press.
- Aït-Sahalia, Yacine, Per A Mykland, and Lan Zhang (2005). “How often to sample a continuous-time process in the presence of market microstructure noise”. In: *The review of financial studies* 18.2, pp. 351–416.
- Aït-Sahalia, Yacine and Dacheng Xiu (2019). “A Hausman test for the presence of market microstructure noise in high frequency data”. In: *Journal of Econometrics* 211.1, pp. 176–205.
- Almgren, Robert and Neil Chriss (2001). “Optimal execution of portfolio transactions”. In: *Journal of Risk* 3, pp. 5–40.
- Andersen, Torben G, Dobrislav Dobrev, and Ernst Schaumburg (2012). “Jump-robust volatility estimation using nearest neighbor truncation”. In: *Journal of Econometrics* 169.1, pp. 75–93.
- Barndorff-Nielsen, Ole E, Peter Reinhard Hansen, Asger Lunde, and Neil Shephard (2008). “Designing realized kernels to measure the ex post variation of equity prices in the presence of noise”. In: *Econometrica* 76.6, pp. 1481–1536.
- Bouchaud, Jean-Philippe, Julius Bonart, Jonathan Donier, and Martin Gould (2018). *Trades, quotes and prices: financial markets under the microscope*. Cambridge University Press.
- Delbaen, Freddy and Walter Schachermayer (1994). “A general version of the fundamental theorem of asset pricing”. In: *Mathematische annalen* 300.1, pp. 463–520.
- Eisler, Zoltán., Jean-Philippe Bouchaud, and Julien Kockelkoren (2012). “The price impact of order book events: Market orders, limit orders and cancellations”. In: *Quantitative Finance* 12, pp. 1395–1419.
- Fan, Jianqing and Yazhen Wang (2008). “Spot volatility estimation for high-frequency data”. In: *Statistics and its Interface* 1.2, pp. 279–288.
- Figuroa-López, José E and Cheng Li (2020). “Optimal kernel estimation of spot volatility of stochastic differential equations”. In: *Stochastic Processes and their Applications* 130.8, pp. 4693–4720.
- Figuroa-López, José E and Bei Wu (2022). “Kernel estimation of spot volatility with microstructure noise using pre-averaging”. In: *arXiv preprint arXiv:2004.01865*.
- Gatheral, Jim and Roel CA Oomen (2010). “Zero-intelligence realized variance estimation”. In: *Finance and Stochastics* 14.2, pp. 249–283.
- Guéant, Olivier (2016). *The Financial Mathematics of Market Liquidity: From optimal execution to market making*. Vol. 33. CRC Press.
- Hansen, Peter R and Asger Lunde (2006). “Realized variance and market microstructure noise”. In: *Journal of Business & Economic Statistics* 24.2, pp. 127–161.
- Hansen, Peter R, Asger Lunde, and James M Nason (2011). “The model confidence set”. In: *Econometrica* 79.2, pp. 453–497.
- Hasbrouck, Joel (2007). *Empirical market microstructure: the institutions, economics, and econometrics of securities trading*. Oxford University Press.

- Huang, Weibing, Charles-Albert Lehalle, and Mathieu Rosenbaum (2015). “Simulating and analyzing order book data: The queue-reactive model”. In: *Journal of the American Statistical Association* 110.509, pp. 107–122.
- Jacod, Jean, Yingying Li, Per A Mykland, Mark Podolskij, and Mathias Vetter (2009). “Microstructure noise in the continuous case: The pre-averaging approach”. In: *Stochastic processes and their applications* 119.7, pp. 2249–2276.
- Jing, Bing-Yi, Zhi Liu, and Xin-Bing Kong (2014). “On the estimation of integrated volatility with jumps and microstructure noise”. In: *Journal of Business & Economic Statistics* 32.3, pp. 457–467.
- Kristensen, Dennis (2010). “Nonparametric filtering of the realized spot volatility: A kernel-based approach”. In: *Econometric Theory* 26.1, pp. 60–93.
- Large, Jeremy (2011). “Estimating quadratic variation when quoted prices change by a constant increment”. In: *Journal of Econometrics* 160.1, pp. 2–11.
- Li, Jia, Dishen Wang, and Qiushi Zhang (2022). “Reading the Candlesticks: An OK Estimator for Volatility”. In: *The Review of Economics and Statistics*, pp. 1–45.
- Li, Yingying, Guangying Liu, and Zhiyuan Zhang (2021). “Volatility of volatility: Estimation and tests based on noisy high frequency data with jumps”. In: *Journal of Econometrics*.
- Li, Yingying, Zhiyuan Zhang, and Yichu Li (2018). “A unified approach to volatility estimation in the presence of both rounding and random market microstructure noise”. In: *Journal of Econometrics* 203.2, pp. 187–222.
- Lillo, Fabrizio and J Doynne Farmer (2004). “The long memory of the efficient market”. In: *Studies in nonlinear dynamics & econometrics* 8, p. 3.
- Malliavin, Paul and Maria Elvira Mancino (2002). “Fourier series method for measurement of multivariate volatilities”. In: *Finance and Stochastics* 6.1, pp. 49–61.
- (2009). “A Fourier transform method for nonparametric estimation of multivariate volatility”. In: *The Annals of Statistics* 37.4, pp. 1983–2010.
- Mancini, Cecilia, Vanessa Mattiussi, and Roberto Renò (2015). “Spot volatility estimation using delta sequences”. In: *Finance and Stochastics* 19.2, pp. 261–293.
- Mancino, Maria Elvira and Maria Cristina Recchioni (2015). “Fourier spot volatility estimator: Asymptotic normality and efficiency with liquid and illiquid high-frequency data”. In: *PloS one* 10.9, e0139041.
- Mancino, Maria Elvira and Simona Sanfelici (2008). “Robustness of Fourier estimator of integrated volatility in the presence of microstructure noise”. In: *Computational Statistics & data analysis* 52.6, pp. 2966–2989.
- Ogawa, Shigeyoshi (2008). “Real-time scheme for the volatility estimation in the presence of microstructure noise”. In: *Monte Carlo Methods and Applications* 14.4, pp. 331–342.
- Ogawa, Shigeyoshi and Simona Sanfelici (2011). “An improved two-step regularization scheme for spot volatility estimation”. In: *Economic Notes* 40.3, pp. 107–134.

- Patton, Andrew J (2011). “Volatility forecast comparison using imperfect volatility proxies”. In: *Journal of Econometrics* 160.1, pp. 246–256.
- Robert, Christian Y and Mathieu Rosenbaum (2011). “A new approach for the dynamics of ultra-high-frequency data: The model with uncertainty zones”. In: *Journal of Financial Econometrics* 9.2, pp. 344–366.
- Roll, Richard (1984). “A simple implicit measure of the effective bid-ask spread in an efficient market”. In: *The Journal of finance* 39.4, pp. 1127–1139.
- Smith, Eric, J Doyne Farmer, László Gillemot, and Supriya Krishnamurthy (2003). “Statistical theory of the continuous double auction”. In: *Quantitative finance* 3.6, p. 481.
- Vortelinos, Dimitrios I (2014). “Optimally sampled realized range-based volatility estimators”. In: *Research in International Business and Finance* 30, pp. 34–50.
- Zhang, Lan (2006). “Efficient estimation of stochastic volatility using noisy observations: a multi-scale approach”. In: *Bernoulli* 12.6, pp. 1019–1043.
- Zhang, Lan, Per A Mykland, and Yacine Aït-Sahalia (2005). “A tale of two time scales: Determining integrated volatility with noisy high-frequency data”. In: *Journal of the American Statistical Association* 100.472, pp. 1394–1411.
- Zhou, Bin (1996). “High-frequency data and volatility in foreign-exchange rates”. In: *Journal of Business & Economic Statistics* 14.1, pp. 45–52.
- Zu, Yang and H Peter Boswijk (2014). “Estimating spot volatility with high-frequency financial data”. In: *Journal of Econometrics* 181.2, pp. 117–135.

Appendix A

A.1 Additional performance results (variable θ and θ^{reinit})

A.1.1 5 regimes

Integrated variance estimators - relative bias							
Estimator	mid-price	rank	micro-price	rank	trade-price	rank	av. rank
Pre-averaging	0.02365	1	0.02519	1	0.02364	1	1
Med RV	-0.03787	2	-0.03778	2	-0.03738	2	2
Min RV	-0.03828	3	-0.03821	3	-0.03782	3	3
Range	-0.07194	4	-0.05015	4	-0.06590	4	4
Unified	0.092375	5	0.08478	5	0.16468	7	6
Fourier	0.12680	7	0.10451	6	0.12580	6	6.33
Alternation	0.09803	6	0.19524	12	0.09607	5	7.66
Kernel	0.17164	9	0.14899	8	0.31278	8	8.33
Maximum likelihood	0.16986	8	0.14813	7	0.41152	11	8.66
Two-scale RV	0.17577	10	0.15552	9	0.41140	9	9.33
Multi-scale RV	0.17592	11	0.15569	10	0.41152	10	10.33
Bias-corrected RV	0.17606	12	0.15583	11	0.41164	12	11.66

Table 15: Performance and ranking of the integrated variance estimators for the series of mid-price, micro-price and trade-price with 5 regimes of θ and θ^{reinit} , according to the relative bias. The average ranking is reported in the last column.

Integrated variance estimators - relative MSE							
Estimator	mid-price	rank	micro-price	rank	trade-price	rank	av. rank
Unified	0.01002	1	0.00864	1	0.02881	7	3
Fourier	0.01525	3	0.01251	2	0.01823	4	3
Range	0.01769	4	0.01253	3	0.01029	2	3
Pre-averaging	0.01888	5	0.01691	4	0.01685	3	4
Alternation	0.01020	2	0.03927	12	0.00332	1	5
Med RV	0.02022	6	0.02022	5	0.02010	5	5.33
Min RV	0.02511	7	0.02510	8	0.02492	6	7
Maximum likelihood	0.03008	8	0.02311	6	0.12163	9	7.66
Kernel	0.03075	9	0.02334	7	0.10014	8	8
Two-scale RV	0.03211	10	0.02534	9	0.17089	10	9.66
Multi-scale RV	0.032161	11	0.02539	10	0.17098	11	10.66
Bias-corrected RV	0.03222	12	0.02543	11	0.17102	12	11.66

Table 16: Performance and ranking of the integrated variance estimators for the series of mid-price, micro-price and trade-price with 5 regimes of θ and θ^{reinit} , according to the relative mean square error. The average ranking is reported in the last column.

Spot variance estimators - relative integrated bias							
Estimator	mid-price	rank	micro-price	rank	trade-price	rank	av. rank
Fourier	-0.00099	1	-0.00083	1	-0.00597	1	1
Regularized	-0.00904	2	-0.00912	2	-0.00877	2	2
Pre-averaging kernel	-0.06324	3	-0.04842	3	-0.05288	3	3
Optimal candlestick	-0.16978	4	-0.12938	4	-0.07699	4	4
Pre-averaging	0.17632	5	0.17629	5	-0.11810	5	5
Kernel	0.20633	6	0.26122	6	0.27361	6	6
Two-scale	-0.24749	7	0.26543	7	0.81305	7	7

Table 17: Performance and ranking of the spot variance estimators for the series of mid-price, micro-price and trade-price with 5 regimes of θ and θ^{reinit} , according to the relative integrated bias. The average ranking is reported in the last column.

Spot variance estimators - relative integrated MSE							
Estimator	mid-price	rank	micro-price	rank	trade-price	rank	av. rank
Fourier	0.035801	1	0.03585	1	0.03616	1	1
Pre-averaging kernel	0.19077	2	0.19206	2	0.14159	2	2
Regularized	0.21590	3	0.21592	3	0.21582	3	3
Optimal candlestick	0.31354	4	0.31110	4	0.32879	4	4
Kernel	0.42691	5	0.49152	5	0.82784	5	5
Two-scale	1.62405	6	1.61549	6	2.38642	6	6
Pre-averaging	2.52237	7	2.52255	7	2.52422	7	7

Table 18: Performance and ranking of the spot variance estimators for the series of mid-price, micro-price and trade-price with 5 regimes of θ and θ^{reinit} , according to the relative integrated mean square error. The average ranking is reported in the last column.

A.1.2 10 regimes

Integrated variance estimators - relative bias							
Estimator	mid-price	rank	micro-price	rank	trade-price	rank	av. rank
Med RV	0.06614	1	0.06609	1	0.06660	1	1
Pre-averaging	0.07184	2	0.07182	2	0.07237	2	2
Min RV	0.07669	3	0.07667	3	0.07680	4	3.33
Range	-0.12325	5	-0.11637	5	0.13146	5	5
Unified	0.12626	6	0.11419	4	0.19885	7	5.66
Fourier	0.16911	7	0.14236	6	0.17286	6	6.33
Alternation	0.09319	4	0.16445	12	-0.0741	3	6.33
Maximum likelihood	0.18492	8	0.15720	7	0.37057	9	8
Kernel	0.18758	10	0.15928	8	0.34518	8	9
Two-scale RV	0.18740	9	0.16030	9	0.43099	10	9.33
Multi-scale RV	0.18759	11	0.16048	10	0.43118	11	10.66
Bias-corrected RV	0.18773	12	0.16061	11	0.43131	12	11.66

Table 19: Performance and ranking of the integrated variance estimators for the series of mid-price, micro-price and trade-price with 10 regimes of θ and θ^{reinit} , according to the relative bias. The average ranking is reported in the last column.

Integrated variance estimators - relative MSE							
Estimator	mid-price	rank	micro-price	rank	trade-price	rank	av. rank
Unified	0.01742	2	0.01447	1	0.04113	7	3.33
Fourier	0.02189	3	0.02270	2	0.03208	5	3.33
Range	0.02660	4	0.02659	4	0.02070	2	3.33
Alternation	0.01003	1	0.02796	11	0.00111	1	4.33
Pre-averaging	0.02732	5	0.02632	5	0.02734	3	4.33
Maximum likelihood	0.03541	7	0.02586	3	0.13900	9	6.33
Med RV	0.02881	6	0.02712	10	0.02987	4	6.66
Kernel	0.03641	10	0.02655	6	0.12112	8	8
Min RV	0.03572	8	0.03674	12	0.03674	6	8.66
Multi-scale RV	0.03639	9	0.02689	8	0.18767	10	9
Two-scale RV	0.03642	11	0.02684	7	0.18770	11	9.66
Bias-corrected RV	0.03645	12	0.02694	9	0.18779	12	11

Table 20: Performance and ranking of the integrated variance estimators for the series of mid-price, micro-price and trade-price with 10 regimes of θ and θ^{reinit} , according to the relative mean square error. The average ranking is reported in the last column.

Spot variance estimators - relative integrated bias							
Estimator	mid-price	rank	micro-price	rank	trade-price	rank	av. rank
Fourier	-0.02342	1	-0.02412	1	-0.01745	1	1
Regularized	-0.02472	2	-0.02471	2	-0.02438	2	2
Pre-averaging kernel	-0.08816	3	-0.09235	3	-0.07796	3	3
Optimal candlestick	-0.20641	5	-0.15948	4	-0.0838	4	4.33
Pre-averaging	0.24979	6	0.24976	5	0.24958	5	5.33
Kernel	0.20568	4	0.25983	6	0.79978	6	5.66
Two-scale	-0.27408	7	-0.28400	7	-0.28864	7	7

Table 21: Performance and ranking of the spot variance estimators for the series of mid-price, micro-price and trade-price with 10 regimes of θ and θ^{reinit} , according to the relative integrated bias. The average ranking is reported in the last column.

Spot variance estimators - relative integrated MSE							
Estimator	mid-price	rank	micro-price	rank	trade-price	rank	av. rank
Fourier	0.05523	1	0.05527	1	0.05618	1	1
Pre-averaging kernel	0.19695	2	0.19833	2	0.15153	2	2
Regularized	0.23490	3	0.23502	3	0.23458	3	3
Optimal candlestick	0.31762	4	0.31529	4	0.34982	4	4
Kernel	0.57819	5	0.68831	5	0.79963	5	5
Two-scale	1.61446	6	1.65113	6	2.78745	7	6.33
Pre-averaging	2.49265	7	2.49293	7	2.49131	6	6.66

Table 22: Performance and ranking of the spot variance estimators for the series of mid-price, micro-price and trade-price with 10 regimes of θ and θ^{reinit} , according to the relative integrated mean square error. The average ranking is reported in the last column.

A.2 Sample daily volatility trajectories of spot variance estimates (micro-price and trade-price)

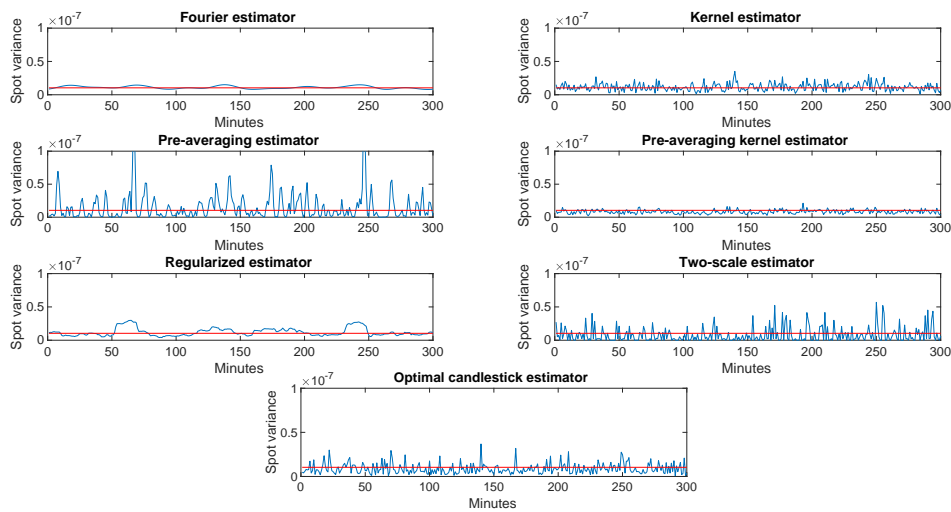


Figure 4: Constant θ and θ^{reinit} : sample trajectories of spot variance estimators computed from micro-prices (in blue) and true volatility (in red).

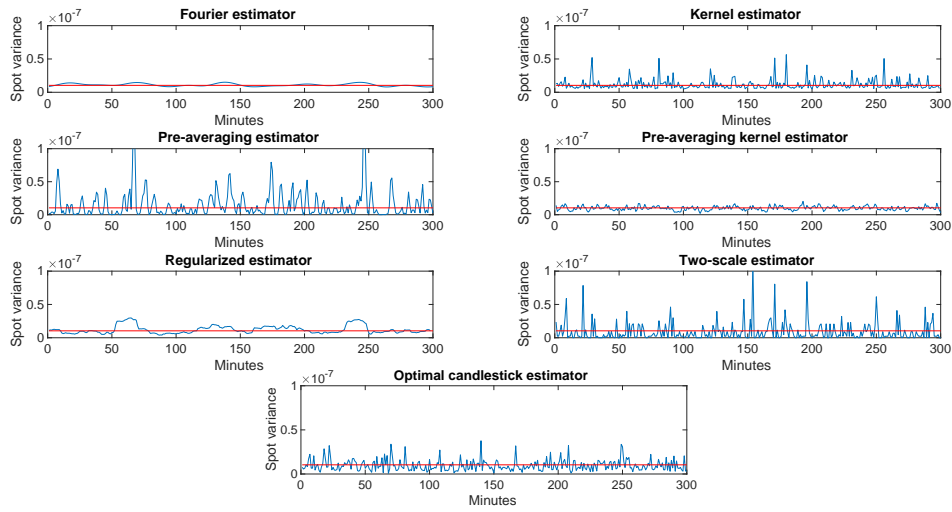


Figure 5: Constant θ and θ^{reinit} : sample trajectories of spot variance estimators computed from trade-prices (in blue) and true volatility (in red).

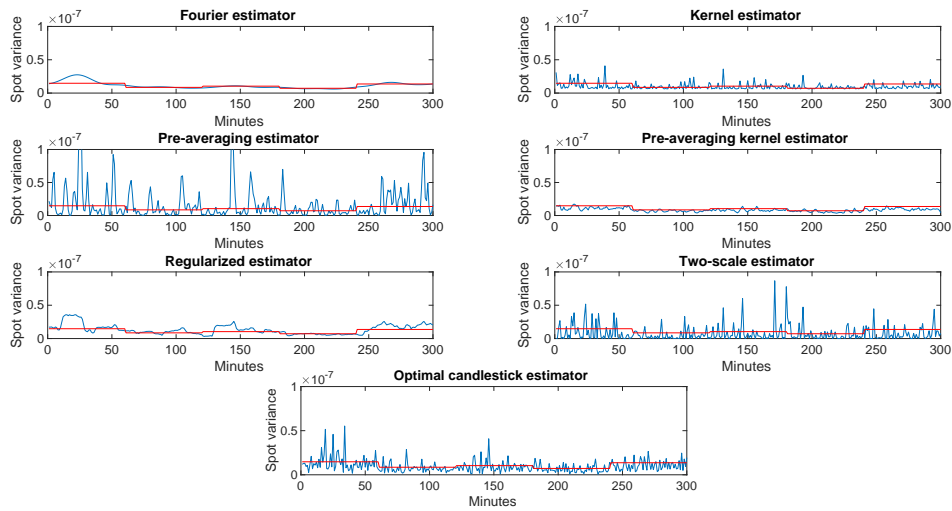


Figure 6: Variable θ and θ^{reinit} (5 regimes): sample trajectories of spot variance estimators computed from micro-prices (in blue) and true volatility (in red).

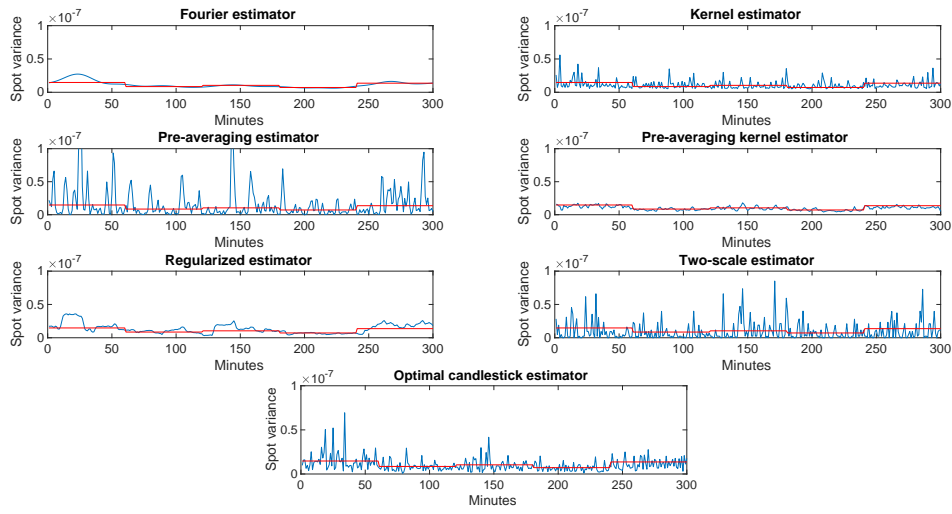


Figure 7: Variable θ and θ^{reinit} (5 regimes): sample trajectories of spot variance estimators computed from trade-prices (in blue) and true volatility (in red).

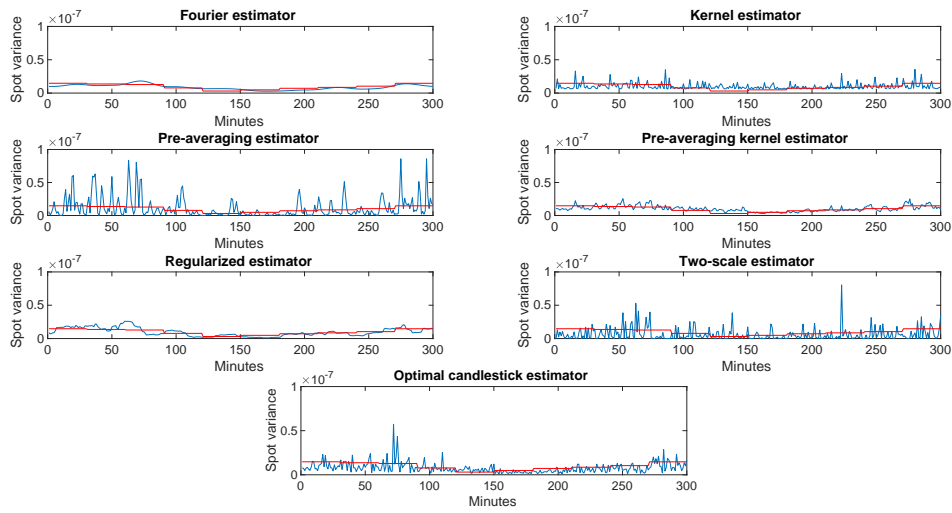


Figure 8: Variable θ and θ^{reinit} (10 regimes): sample trajectories of spot variance estimators computed from micro-prices (in blue) and true volatility (in red).

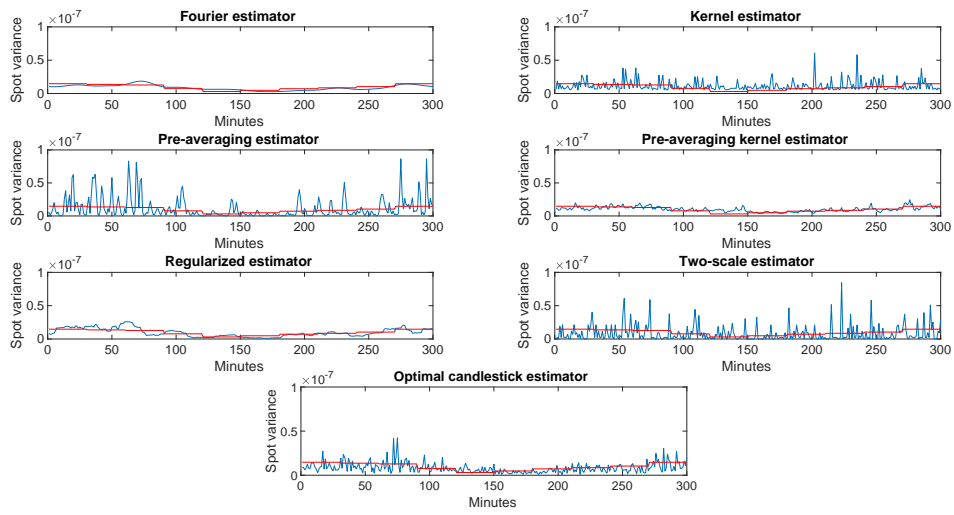


Figure 9: Variable θ and θ^{reinit} (10 regimes): sample trajectories of spot variance estimators computed from trade-prices (in blue) and true volatility (in red).